Annals of Glaciology

Article

Cite this article: Carter CM, Franke S, Paxman GJG, Jamieson SSR, Bentley MJ, Jansen D, Paden J, Eisen O (2025) Topographic and geologic controls on the Northeast Greenland Ice Stream. *Annals of Glaciology* **66**, e29, 1–14. https://doi.org/10.1017/aog.2025.10028

Received: 30 June 2025
Revised: 6 October 2025
Accepted: 20 October 2025

Keywords:
glacial geomorphology; ice streams; radio-echo sounding

Corresponding author: Charlotte M. Carter; Email: charlotte.carter@awi.de

cambridge.org/aog

Topographic and geologic controls on the Northeast Greenland Ice Stream

Charlotte M. Carter[1,2], Steven Franke[3], Guy J.G. Paxman[4], Stewart S.R. Jamieson[4], Michael J. Bentley[4], Daniela Jansen[1], John Paden[5] and Olaf Eisen[1,2]

[1]Alfred-Wegener-Institut Helmholtz-Zentrum für Polar- und Meeresforschung, Bremerhaven, Germany; [2]Fachbereich Geowissenschaften, Universität Bremen, Bremen, Germany; [3]Fachbereich Geowissenschaften, Universität Tübingen, Tübingen, Germany; [4]Department of Geography, Durham University, Durham, UK and [5]Center for Remote Sensing and Integrated Systems, University of Kansas, Lawrence, KS, USA

Abstract

The Northeast Greenland Ice Stream (NEGIS) is an elongated feature extending ~600 km into the interior of the Greenland Ice Sheet. Here, we investigate detailed subglacial topography along the length of the NEGIS to ascertain the characteristics of the ice stream bed. We use topographic analysis (hypsometry, spatial roughness and valley morphometry) to describe and demarcate three geomorphologically distinct regions. The upstream region, near the NEGIS onset, exhibits low roughness and a lack of valleys, indicating the likely presence of subglacial sediments. Downstream, roughness abruptly increases, with two wide subglacial troughs present in the middle region. In the downstream region, the topography displays smaller alpine-like valleys. We propose that these differences are attributable to changing geological provinces, which are poorly constrained in this area. The topography also has a distinct impact on ice stream geometry, as ice flow is generally preferentially steered through a trough. Whilst the upstream regime appears to have little effect on the location of the ice stream onset and shear margins, its low friction enables fast flow that propagates longitudinally upstream from the troughs. On the basis of our data, we argue that the NEGIS is more strongly influenced by basal topography than has been previously suggested.

1. Introduction

Approximately 17% of the present-day Greenland Ice Sheet is drained via the Northeast Greenland Ice Stream (NEGIS) (Krieger and others, 2019), which extends ~600 km into the interior, reaching almost to the ice divide. The NEGIS is generally thought to be topographically unconstrained (Christianson and others, 2014; Holschuh and others, 2019; Franke and others, 2020), as the onset of fast-flowing ice is not confined to, or channelled by, a distinct valley or trough. Similarly unconstrained ice streams in Greenland, such as Petermann Glacier, however, exhibit convergent flow into a main trunk (Chu and others, 2018) and lack the clearly defined shear margins that make the NEGIS unique in its geometry.

The complex nature of the NEGIS has given rise to various theories about the onset of its fast flow so far into the interior of Greenland. For example, the NEGIS has been thought to originate as a result of high geothermal heat flux beneath the onset zone (Fahnestock and others, 2001; Rysgaard and others, 2018). However, modelling of this potential geothermal hotspot in order to initiate and sustain the NEGIS has provided unrealistically high values of geothermal heat flux (Smith-Johnsen and others, 2020), leading to this theory being disputed (Bons and others, 2021). The presence of water-saturated dilatant till has also been proposed to facilitate ice stream flow, suggesting a control through subglacial water routing (Christianson and others, 2014). Other work ascribes the characteristics of the ice stream to the interaction of ice crystal fabric anisotropy and dynamics (Gerber and others, 2023), where the crystal orientation fabric considerably affects the ice stiffness at the onset of the NEGIS. Knowledge of the stability and recent dynamics of the ice stream has also evolved. Originally thought to likely be a steady state feature of the ice sheet (Joughin and others, 2001), the current NEGIS has been shown to be a relatively young, transitory ice stream, where the shear margins have only consolidated 2000 years ago (Jansen and others, 2024), sometime after major deglaciation following the Last Glacial Maximum (Roberts and others, 2024) and subsequent drainage basin reconfiguration throughout the Holocene (Franke and others, 2022a).

More widely, multiple factors can potentially influence the location of an ice stream and the onset of its fast flow, for instance, topographic focusing or sudden changes in bed gradient, basal roughness, subglacial geology, geothermal heat flux and subglacial water routing (Winsborrow and others, 2010). In the absence of a strong topographic control, ice streams

preferentially occur where basal stresses are lower, that is, where subglacial meltwater routing and geology are favourable, after which bed roughness, geothermal heat flux and topographic steps are thought to be the next most important controls (Winsborrow and others, 2010). It has also been proposed that a relationship, although not directly causal, exists between faster ice flow and decreased basal roughness in Antarctic ice streams (Rippin and others, 2011, 2014); however, fast ice flow can also occur over a rough, hard bed (Falcini and others, 2018).

In the case of the NEGIS, basal roughness evolves downstream, changing from a smooth bed at the onset, to a rougher bed where the ice stream widens, correlating with the slowing of the ice stream and lateral variations in the ice surface velocity (Franke and others, 2021). Subglacial water routing has also been established to play a significant role in the ice stream, through the reduction of basal shear stress and facilitation of basal slip (Joughin and others, 2001; Karlsson and Dahl-Jensen, 2015; Franke and others, 2021), whereas the subglacial geology is poorly constrained. The delineation of subglacial geological boundaries across Greenland has been determined from a synthesis of geophysical datasets by MacGregor and others (2024); however, the regions underlying the NEGIS have been highlighted as ones where the subglacial geology is highly uncertain.

Despite the acquisition of large amounts of bed elevation data across Greenland in recent years (MacGregor and others, 2021), the subglacial topography of the NEGIS has yet to be fully characterised, aside from the more focused studies of Franke and others (2020; 2021). In our study, we aim to investigate the subglacial topography along a length of approximately 400 km of the NEGIS from its onset to its divergence into outlet glaciers, in order to ascertain the characteristics of the subglacial conditions over which the NEGIS flows. We examine how the variations in topography beneath the NEGIS are related to ice flow, as well as whether there is an evident geological signal that would impact the subglacial topography. Therefore, we use a geomorphometric approach, utilising the metrics of hypsometry, spatial topographic roughness and valley morphometry, to improve our understanding of how or if topography is exerting a control on the NEGIS, as well as other processes such as geology or hydrology, which may leave topographic signals.

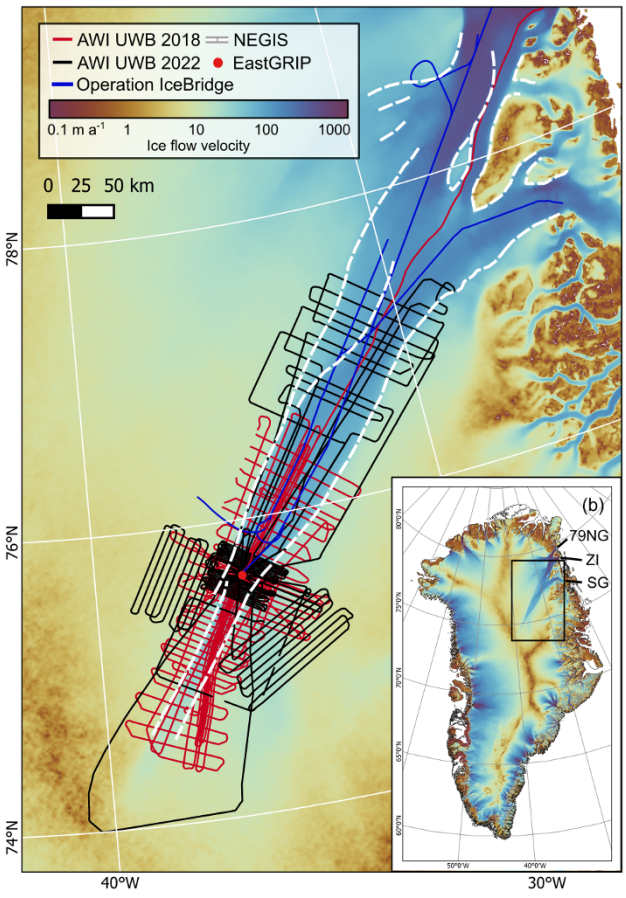

Figure 1. (a) Surface velocity map (Gardner and others, 2022) of the northeastern section of the Greenland Ice Sheet, highlighting the NEGIS. The shear margins of the ice stream are highlighted, drawn where there is a sharp change in the velocity gradient (white dashes). The flightlines of the AWI surveys (Franke and others, 2019; Carter and others, 2023) and selected lines from Operation IceBridge surveys (CReSIS, 2024a) (black, red and blue lines) are centred around the EastGRIP ice core site, and span from the onset to where the ice stream diverges into multiple outlets. (b) Inset map shows the surface velocity of the Greenland Ice Sheet, with the outlet glaciers of NEGIS labelled (79NG, ZI, and SG).

2. Data and methods

In this section, we first describe the airborne radio-echo sounding (RES) data utilised in this study, and the subsequent derivation of ice thickness and bed elevation to produce an updated version of the BedMachine digital elevation model (Morlighem and others, 2017). We then use these datasets to elucidate the characteristics of the subglacial topography, through hypsometric analysis, spatial topographic roughness and valley morphometrics.

2.1. Airborne RES data

We use the airborne RES data of the EGRIP-NOR-2018 and NEGIS-FLOW-2022 surveys (Franke and others, 2019; Carter and others, 2023) (Fig. 1), which span from the onset area of the NEGIS to the divergence of the ice stream into its three outlet glaciers: Nioghalvfjerdsfjord Glacier (79NG), Zacharie Isstrøm (ZI) and Storstrømmen Glacier (SG). The EGRIP-NOR-2018 survey covers the EastGRIP ice core site with a line spacing of 5 km, with 10 km spacing further up- and downstream (Franke and others, 2020) and flightlines oriented both perpendicular and sub-parallel to ice-flow direction. This survey was subsequently extended by NEGIS-FLOW-2022, which added downstream flightlines at spacings of 6–25 km, to cover a total area of ~46,000 km^2, reaching 200 km upstream and 260 km downstream of the core site.

These data were collected with the Alfred Wegener Institute (AWI) multi-channel ultra-wideband (UWB) airborne radar sounder, mounted on the Polar6 aircraft (Alfred-Wegener-Institut Helmholtz-Zentrum für Polar- und Meeresforschung, 2016), with a centre frequency of 195 MHz and bandwidth of 30 MHz. A detailed description of AWI's UWB radar system is given by Rodriguez-Morales and others (2014); Hale and others (2016); and Arnold and others (2020), as well as a methodological description of the data acquisition and processing in Franke and others (2020) and Franke and others (2022b). Additional selected RES data, aligned with the flightline direction of the AWI surveys, were obtained from Operation IceBridge (OIB) (CReSIS, 2024a) (Fig. 1) in order to expand the area of analysis within the survey region.

2.2. Derivation of bed topography

The surface and bed reflection of the RES data were delineated using the seismic processing and interpretation software

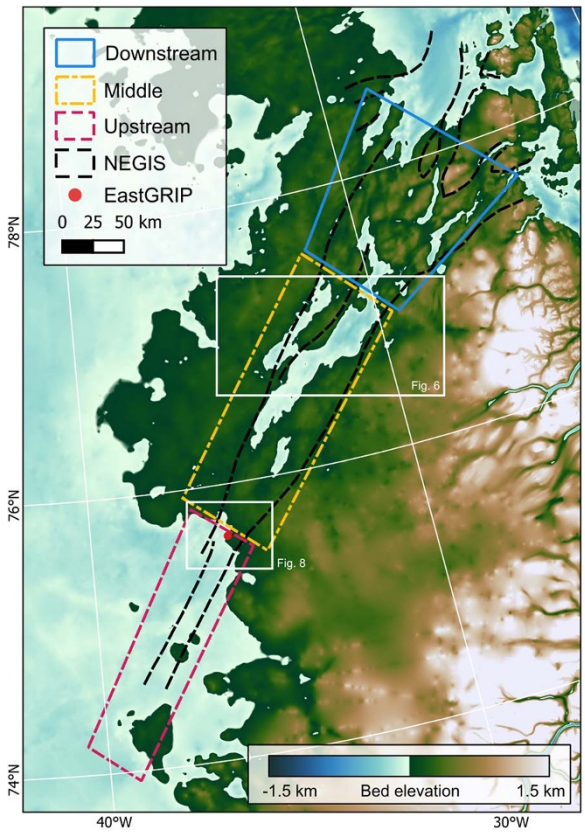

Figure 2. (a) Subglacial topography (Morlighem and others, 2017) beneath the NEGIS, divided into three regions: upstream, middle and downstream.

Paradigm™ by Aspen Technology Inc. To convert from two-way travel time to ice thickness, we used an ordinary relative dielectric permittivity of 3.15. Thicknesses were then subtracted from the GIMP DEM surface elevation model (Howat and others, 2014) to calculate bed elevation. Surface elevation measurements derived from the aircraft's laser altimeter were not utilised in order to make the method reproducible and consistent with other datasets. A crossover analysis was performed in order to ascertain the range uncertainty across the bed picks, as described in Franke and others (2020), which takes the root mean square errors of the range resolution and dielectric constant. For our ice thickness values ranging between ~1000–3300 m, the mean crossover deviation is 12.23 m. The bed elevation point data from NEGIS-FLOW-2022 were integrated into a new version of BedMachine (v6.2, Fig. 2) (Morlighem and others, 2017), which showed clear differences in the representation of the trough edges as compared to BedMachine v5 (Appendix A, Fig. A1).

From this new bed topography dataset, the study area was divided into three regions of similar morphology (Fig. 2). The upstream region encompasses the onset of the ice stream upstream of the EastGRIP ice core site and is characterised by lower elevation topography with flatter relief. Moving downstream, the middle region can be delineated from an upward step in the subglacial topography (~300 m) situated immediately downstream of EastGRIP. It is characterised by large, broad and shallow subglacial troughs which trend parallel to modern ice flow. The transition from the middle to the downstream region occurs where there is a shift to a more alpine appearance of the topography, where the relief of the topography is higher.

2.3. Hypsometric analysis

In order to analyse the frequency distribution of elevations across the study area, hypsometric curves were calculated from BedMachine v6.2. The hypsometry was derived for each region (Fig. 2), as the percentage distribution of elevations. The distribution of elevations within an area can highlight the dominance of particular processes within a landscape (Jamieson and others, 2014). For example, the presence of troughs cut to a particular elevation would result in a distinctive peak in the hypsometry, as the flat floor of a trough relates to a large percentage of the bed, which is situated in a particular elevation band.

2.4. Spatial topographic roughness

We use the bed elevation point data from the AWI 2018 and 2022 surveys, as well as selected survey lines from OIB (Fig. 1), for our basal roughness calculations. We evaluate spatial topographic roughness using the standard deviation of vertical change in bed elevation over a given horizontal distance (root mean square height [RMSh]) (Rippin and others, 2006). A rougher bed is represented by a higher RMSh, as it implies a greater spread between higher and lower elevations (Falcini and others, 2018).

For each data point on a linearly detrended profile, we calculated RMSh using a moving window size of 960 m (64 data points), in order to investigate the effects of small-scale (sub-kilometre) topography. The along-track resolution of all flightlines was ~15 m, meaning that resampling was not required to achieve a constant point spacing. However, if data gaps along the flightlines were present due to missing bed picks, for example, RMSh values were omitted from the analysis as the point spacing was no longer consistent. As the interpretation of roughness parameters is highly directionally dependent (Rippin and others, 2014; Falcini and others, 2018, 2021; Eisen and others, 2020), the analysis of the topographic roughness is divided into across- and along-flow profiles.

Anisotropy, or directionality, of topographic roughness quantifies the difference between roughness parallel and orthogonal to ice flow (Smith, 2014). This can be applied to bed elevation roughness data at points where along- and across-flow profiles intersect, as described in Falcini and others (2021), where the ratio of these roughness parameters was calculated following Smith and others (2006). The value of the anisotropy ratio is closer to −1 when across-flow roughness is higher than along-flow, is 0 when roughness is isotropic, and is closer to 1 when along-flow roughness is higher than across-flow. Values of anisotropy calculated where the bed has elongated bedforms, such as MSGLs or megagrooves, would therefore tend towards −1, as the bed is being streamlined and reducing the roughness parallel to ice flow. Areas with mixed landforms, for example, drumlins or cnoc-and-lochan terrain, would demonstrate more isotropic values (Falcini and others, 2021). In the context of ice streams, elongated landforms and smoother surfaces can infer either deformable sediment or a smooth bedrock surface which can be preferentially eroded. Rougher topography, in contrast, may infer a bedrock interface where the erosional patterns are more isotropic in terms of its fracture and joints, and glacial erosion is less able to be reinforced in the same place (Falcini and others, 2021). The RMSh values at each

intersection of two flightlines were used to calculate this anisotropy ratio.

2.5. Valley morphometrics and classification

The morphology of valley cross-sectional profiles was analysed utilising the workflow of Paxman (2023), which extracted valley profiles from the 2018 and 2022 AWI RES surveys, as well as a wider selection of all OIB survey lines within the study area (Greenland_P3 surveys from 1997, 1999, 2002, 2007, 2010, 2012, 2013, 2014 and 2015) (CReSIS, 2024b). As valley cross-sectional profiles in RES data may be oblique to its ideal orthogonal profile, this effect was corrected for by determining the angular difference between the azimuth of the flightline and the valley strike (perpendicular to valley orientation), as determined from BedMachine v5 (Paxman, 2023). A trigonometric correction was used to adjust the profile as if the survey had been flown orthogonal to the valley orientation, but if the difference between the flightline azimuth and valley strike was >60°, the valley was removed from the analysis. Morphometric indices relating to valley depth, top width, V-index and curvature ratio were calculated for each profile in order to produce quantitative characteristic metrics. Valley cross-profile form is a useful approach in the context of understanding a glaciated landscape, as the morphometry of a valley is characteristic of glacially eroded (*U*-shaped) or fluvially eroded (*V*-shaped) valleys, and can be utilised to distinguish between them. These indices were compared using a random forest classifier to a training dataset of fluvial and glacial valleys elsewhere on Earth, from which a classification score was assigned to each valley, ranging from 0 (most akin to fluvial) to 1 (most akin to glacial). Our analysis focused only on valleys with scores of <0.25 or >0.75, as these reflect 'higher confidence' classifications. The valleys were also compared in terms of their width/depth (W/D) ratios, in order to differentiate between broad, shallow valleys and relatively narrower and deeper valleys, which may have different mechanisms of formation or different geological conditions (Fig. 3).

2.6. Isostatic rebounding of topography

To ascertain the elevations at which pre-glacial topography would reside, the bed topography was isostatically rebounded relative to a hypothetical ice-free world sea level, calculated as caused by the removal of the modern ice sheets without adjustment for thermosteric or ocean dynamical effects (Paxman and others, 2022a). The topography change resulting from ice-sheet unloading was added to BedMachine v6.2 (Paxman and others, 2022b), and a second set of (rebounded) hypsometric curves was calculated as the percentage distribution of elevations (Fig. 5), as detailed above. This analysis was carried out to investigate the potential formational processes of the landscape, as the relative elevations of the pre-glacial topography to sea level can give indications of marine influence, or lack thereof.

3. Results

The subglacial topography of the NEGIS can be divided into three geomorphologically distinct regions (upstream, middle and downstream, outlined in Fig. 2), which are characterised by distinct patterns of spatial topographic roughness, hypsometry, and valley morphometry.

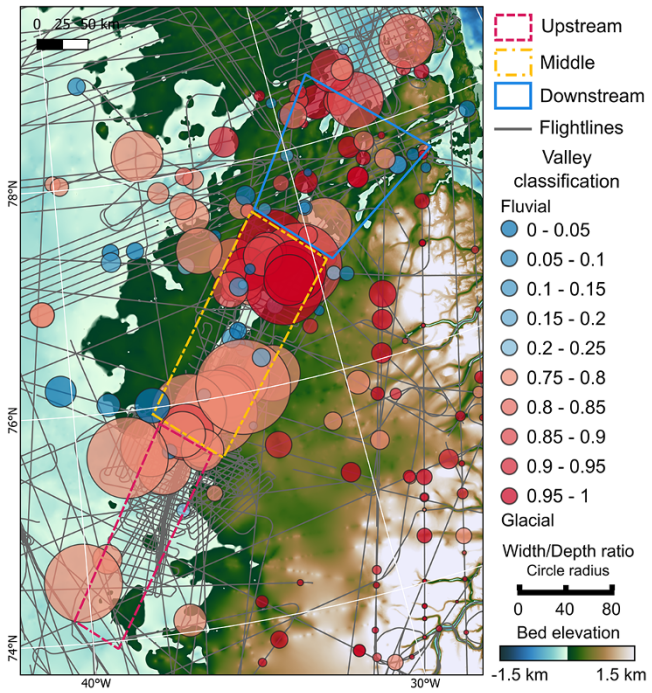

Figure 3. Morphometric classification of valley profiles identified from AWI and Operation IceBridge RES surveys. Colour scale relates to the classification of more fluvial (0, blue) to more glacial (1, red). Circle size represents the W/D ratio of each valley profile (see radius given in legend).

3.1. Upstream region

The topographic region upstream of the EastGRIP ice core site (Fig. 2) underlies the onset zone of the NEGIS, where the ice flow velocity begins to accelerate to ~50 m a^{-1} within the shear margins of the ice stream. The topography here is low elevation (ranging from −300 to 200 m, Fig. 4a), with the majority lying below sea level, sloping slightly inland. A few isolated topographic high points are present, spanning approximately 10–30 km across, however the overall relief is relatively low and smooth. The narrower range of elevations within the hypsometric distribution (432 m, from 5th to 95th percentile) (Fig. 4a) indicates that there is little topographic variation within this region compared with that further downstream. Smaller peaks within the hypsometric curve can be attributed to a shallow topographic low point and low-relief hills. Few valleys (29 profiles) were identified within this region (Fig. 3), all with shallow depths ranging between 102–187 m, thus suggesting that the bed is not strongly incised near the NEGIS onset.

In the isostatically rebounded topography, which represents how the elevations would change with the ice sheet completely removed, the entire study area rebounds above sea level (Fig. 4). The range of elevations for the upstream region shifts to 400–900 m above sea level, but the hypsometric curve retains a similar shape (i.e. elevations are shifted near-uniformly across the region) (Fig. 4a). After isostatic rebounding, these elevations align more closely with the middle and downstream regions (Fig. 4a–c), with the main peak of the upstream region now coincident with the main peak of the downstream region, centred at ~600 m above the ice-free world sea level.

In terms of kilometre-scale topographic roughness, in both along- and across-flow directions, the majority (59%) of RMSh

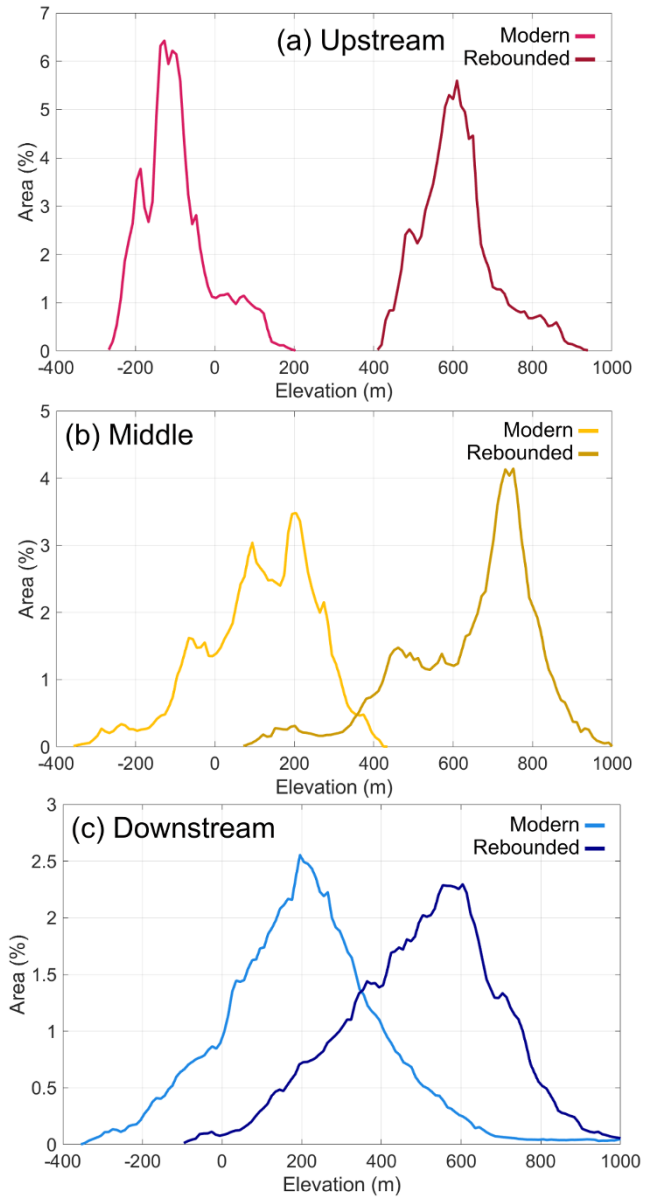

Figure 4. Hypsometric curves of both modern and isostatically rebounded elevations for the (a) upstream, (b) middle and (c) downstream regions. The isostatically rebounded subglacial topography beneath the NEGIS is calculated as if the full ice-sheet load has been removed (Paxman and others, 2022b), the elevations of which are relative to a hypothetical ice-free world sea level.

values are low, between 0–3 m, with no obvious transition in roughness across the shear margins of the ice stream (Fig. 5). Some local higher roughness values are evident over distinct high points in the landscape. In the across-flow direction, a downstream transition to higher roughness values occurs ~25 km upstream of a ~300 m step in the topography at the boundary of the upstream and middle regions. In the along-flow direction, on the western side of the ice stream, the transitional zone can be seen to be more spatially variable. Higher roughness is evident upstream of the topographic step, which decreases moving upstream. The lowest roughness values are contained within the shear margins of the NEGIS (Fig. 5b).

The anisotropy of the spatial roughness is strongly negative surrounding EastGRIP (Fig. 5c), meaning that the roughness across flow is higher than parallel to flow, as the features at the bed are likely longer than they are wide. Outside of the shear margins, more so on the western side, the anisotropy is more isotropic to positive, with limited anisotropy evident very far upstream.

3.2. Middle region

The transition between the upstream and middle region can be delineated almost immediately downstream of EastGRIP, where there is a step of ~300 m in the subglacial topography. The elevations within this middle region range from −400 to 400 m, and the hypsometric curve is negatively skewed with three major peaks (Fig. 4b). Once isostatically rebounded, the hypsometry still demonstrates a strong negative skew, however, the main peak resides at a higher elevation (~750 m) than the main peak of the upstream and downstream regions (Fig. 4b). The region is characterised by two large flow-parallel subglacial troughs, which are evident as the lowest peak in the hypsometric curves of this region (Fig. 4c). The largest of the troughs spans up to 35 km in width and is up to 600 m deep, whilst the smaller trough is ~400 m in depth, and 30 km wide (Fig. 6). Here, the ice stream is widening and increasing in ice flow velocity up to approx. 130 m a^{-1}, and higher ice velocities are focused on the eastern side of the ice stream.

The morphology of the valley profiles in this region would indicate a mix of both 'fluvial' and 'glacial' valleys (Fig. 3). Sixty-nine valley profiles can be identified, however, some of these are consecutive profiles of the same trough, resulting from flightlines crossing multiple times. 'Glacial' valleys here mostly have high W/D ratios (from 8 to 80), meaning that they are relatively wide and shallow, with the highest ratios evident within the largest subglacial trough. 'Fluvial' valleys tend to have lower W/D ratios and are more randomly distributed across the region.

Spatial roughness within the middle region is more variable, with standard deviations of RMSh values of 6.22 m (across-flow) and 4.65 m (along-flow) as compared to the upstream region (3.74 m along-flow and 2.31 m across-flow) (Fig. 5d, e). A distinct, sharp transition to higher roughness values (Fig. 5) is evident at the topographic step that separates the two regions. However, there is no notable lateral difference in roughness across the shear margins in the middle region, as was also the case for the upstream region. In the along-flow direction, areas of low roughness occur most commonly in the topographic lows, or subglacial troughs, with the higher ridges corresponding with higher roughness (Fig. 5b). Across-flow, the largest trough contains a large range of RMSh values from 0.1 to 58.2 m, however, the adjacent trough has a strong signal of high roughness. Further downstream, towards the transition to the downstream region, there is some differentiation in roughness values across the shear margins that can be seen (Fig. 5a). In terms of the roughness anisotropy, stronger negative anisotropy is evident on the topographic highs in the centre of the ice stream, with low to no anisotropy in the deepest parts of the troughs (Fig. 5c).

3.3. Downstream region

Downstream of the large subglacial troughs, the subglacial geomorphology evolves into higher relief topography (Fig. 4c), with a more alpine appearance evidenced by multiple smaller valleys with complex planform geometries (Fig. 2). The valleys have a range of orientations, in contrast to the middle region where the troughs are aligned parallel to ice flow. At this point, the ice stream diverges

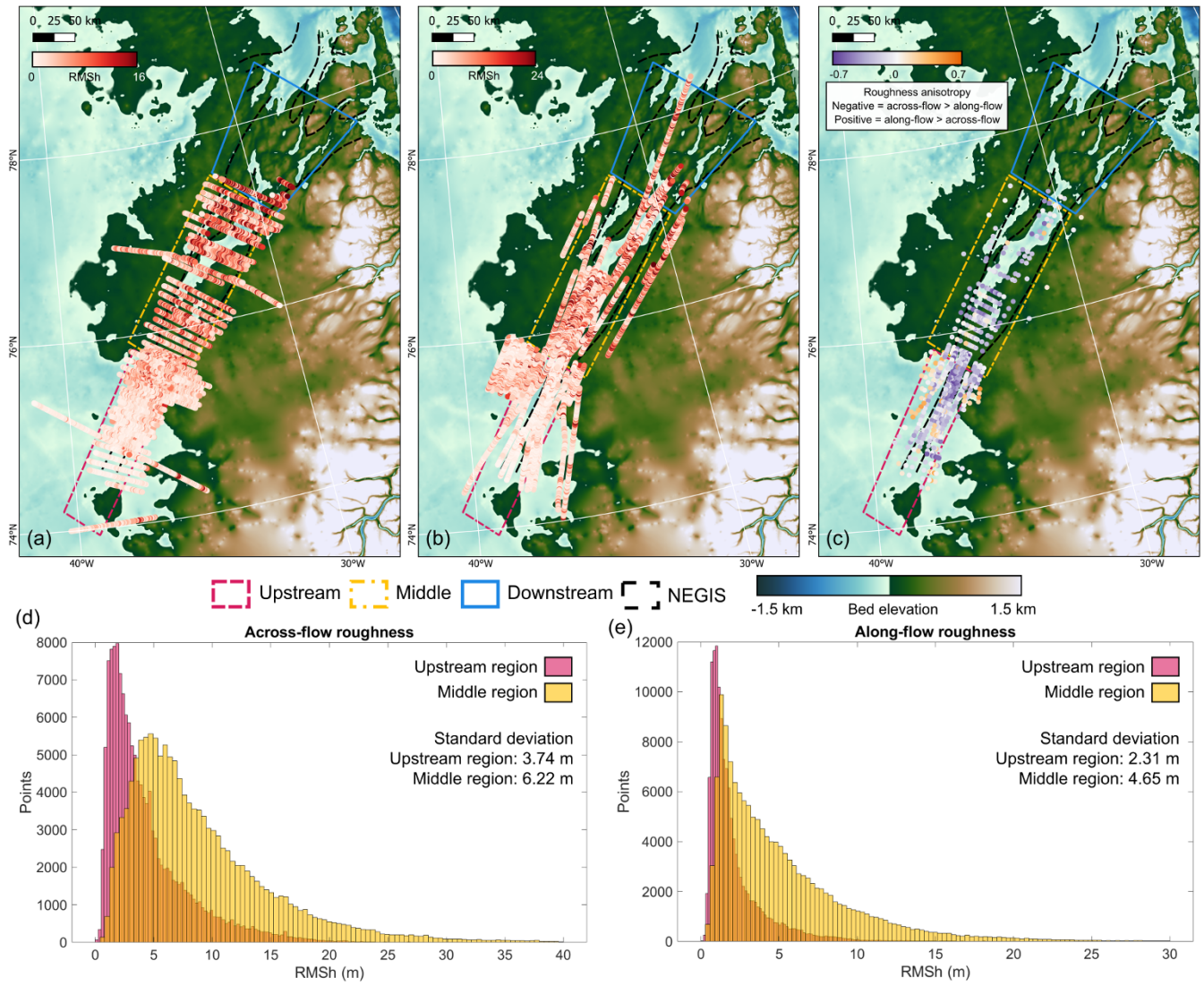

Figure 5. Spatial topographic roughness values (RMSh) calculated using bed elevation point data from AWI and Operation IceBridge RES surveys, separated into (a) across-flow and (b) along-flow flightline orientation. (c) Spatial topographic roughness anisotropy, calculated at the crossing points of perpendicularly oriented flightlines. Values are closer to −1 when across-flow roughness is higher than along-flow, 0 when roughness is isotropic, and closer to 1 when along-flow roughness is higher than across-flow. (d, e) Histograms illustrating the distribution of across- and along-flow RMSh values for the upstream and middle regions.

into its three outlet glaciers (79NG, ZI, and SG), with a noticeable increase in ice flow velocity immediately downstream of this region.

The hypsometric curve for this region demonstrates a unimodal, near-normal histogram, with elevations ranging between −300 to 1000 m (Fig. 4c). Compared to the middle region, the ranges of elevations in terms of major peaks are similar, and the singular peak coincides with the highest elevation peak in the middle region (Fig. 4b, c). The shape of the hypsometric curve remains the same after adjusting for isostatic rebound, but the main peak now sits 400 m higher at 600 m, and the entire region resides above the ice-free sea level (Fig. 4c).

Many 'glacial' valleys can be identified within this region (Fig. 3); however, these have distinctly lower W/D ratios than those in the middle region (ranging between 5–29), meaning that they are relatively narrower and deeper. Some valleys also appear to be channelling the diverging ice stream flow, at the furthest point downstream (Fig. 2). Similarities can also be observed between the valleys identified here and those in the subglacial highlands to the east of the study area, in terms of their highly 'glacial' morphometry and comparable W/D ratios.

Analysis of the spatial roughness within the downstream region is limited, due to the orientation of OIB flightlines not being aligned with ice-flow direction. However, the sparse flightlines that are oriented along the along-flow direction show similar roughness values to the middle region, with some small areas of very low roughness evident in the topographic lows (Fig. 5b).

4. Discussion

The characteristics of the three distinct geomorphological regimes beneath the NEGIS can be clearly differentiated through the changes in hypsometry, spatial roughness and valley morphometry that occur moving progressively downstream from the onset zone (Table 1). The potential origins of the differences between

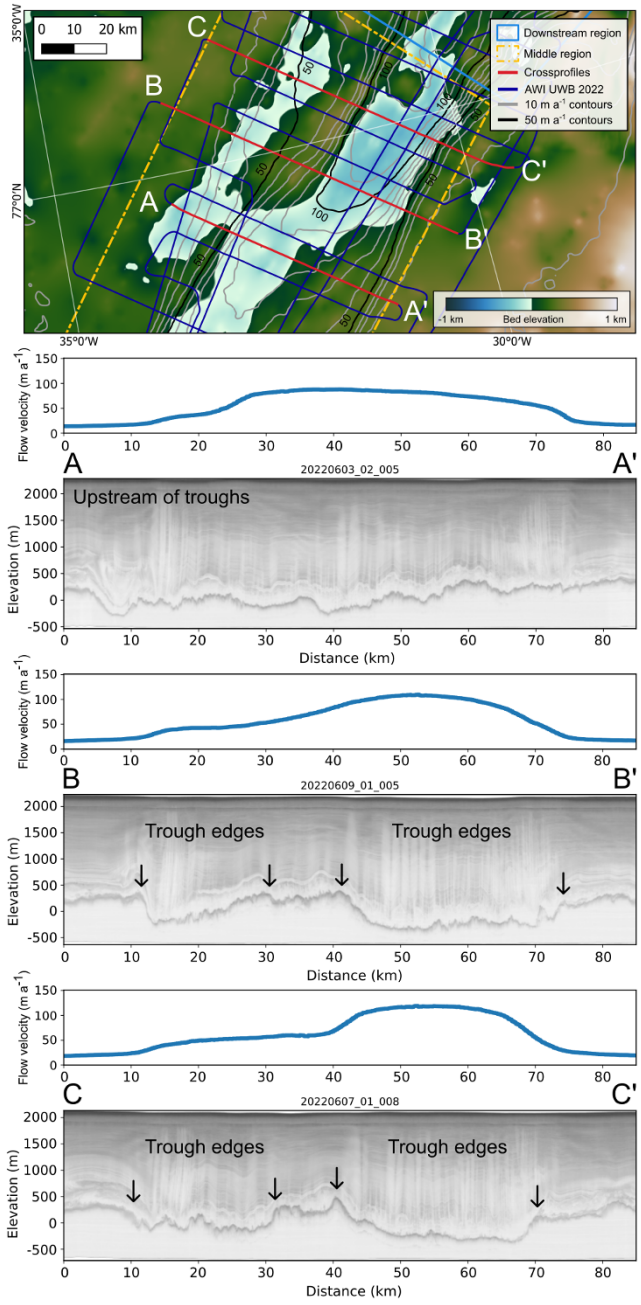

Figure 6. Across-flow radargrams and velocity profiles progressing downstream in the middle region, illustrating the change in surface ice flow velocity (Gardner and others, 2022) towards the east, coinciding with the large subglacial trough. Contour lines of the ice flow velocity are spaced at 50 m a^{-1} (black) and 10 m a^{-1} (grey). Numbers on top of graphs A, B, and C refer to the RES profiles.

these regions, as well as their effects on ice dynamics, are discussed below.

4.1. Origins of the regional geomorphological variability

4.1.1. Upstream region

The region surrounding the onset of the NEGIS is characterised by low roughness values (Fig. 5), an absence of valley incision (Fig. 3), and low relief, which would indicate a likely area of soft sediments (Rippin and others, 2014; Siegert and others, 2016). Parts of

Table 1. Summary of geomorphological characteristics of each region.

	Upstream	Middle	Downstream
Description	Onset of ice stream upstream of EastGRIP. Generally lower elevation, flatter relief topography, with a few topographic highs.	Downstream of upward step in topography at EastGRIP. Characterised by two large flow-parallel subglacial troughs.	Alpine-like topography, with high relief and smaller, variably-oriented valleys.
Hypsometry	Range between −300 to 200 m, positively skewed.	Range between −400 to 400 m, negatively skewed, three peaks.	Range between −300 to 1000 m, unimodal.
Valley morphometry	Few identified valleys.	Mix of both highly glacial and fluvial valleys. Glacial valleys have mostly high W/D ratios, i.e. wide and shallow. Two large overdeepened troughs.	Glacial valleys, but with relatively lower W/D ratios, i.e. narrow and deep. Comparable to those in the eastern subglacial highlands.
Spatial topographic roughness	Majority of very low roughness (0–3 m) in both along- and across-flow directions. Lowest roughness within the shear margin boundaries.	Distinct increase in roughness magnitude and variability immediately downstream of topographic step. Lower roughness within troughs.	Similar roughness values to middle region.

the central area of Greenland have been identified as having low roughness, with sediments potentially being responsible for the observed smooth topography in places (Rippin, 2013; Cooper and others, 2019). In the context of Antarctic ice streams, low roughness has been attributed to the presence of unconsolidated sediments, often marine in origin (Bingham and Siegert, 2007; Rippin and others, 2011, 2014). However, it can also indicate a streamlined hard bed, or exposed crystalline bedrock (Jeofry and others, 2018; Munevar Garcia and others, 2023). Geophysical surveys around the EastGRIP ice core site indicate the presence of saturated sediments (Christianson and others, 2014; Riverman and others, 2019), and sedimentary basins containing MSGLs have been identified beneath the onset zone (Carter and others, 2025). The strongly negative anisotropy of the roughness in this region (Fig. 5c) also corroborates the presence of elongated subglacial features beneath the ice stream (Falcini and others, 2021). Therefore, there are strong indications that the upstream region is underlain by an area of soft sediments, the unconsolidated nature of which suggests a relatively recent origin, rather than a much older Precambrian sedimentary basin.

A possible origin for subglacial sediments is a marine source (Rippin, 2013). Areas situated below sea level could have formerly hosted seaways and been subjected to sediment deposition, as is interpreted to be the case for the region underlying the Siple Coast ice streams in West Antarctica (Studinger and others, 2001). However, when the ice-sheet load is removed from the bed topography of Greenland through isostatic rebounding, the elevations of the interior (including the upstream region described in this study) are significantly above the palaeo-sea level, with the lowest elevations situated at 400 m (Fig. 4a). Even in the case of partial isostatic rebounding, for example, with the presence of an ice cap on the eastern subglacial highlands (Paxman and others, 2024a), there is insufficient subsidence for the elevations of the sediment-covered region to be situated close to or below sea level. Therefore, we rule out a marine origin for these sediments.

A second potential source of sediments within the interior of Greenland could be glacio-lacustrine, resulting from deposition within large proglacial meltwater lakes. The genesis of the Petermann mega-canyon, which spans the interior of Greenland (Bamber and others, 2013), has been posited to have been excavated via repeated catastrophic outburst floods, the mechanism of which also necessitates the presence of large proglacial lakes which occupy the interior (Keisling and others, 2020). The modelled evolution of the ice sheet throughout the Pliocene and Pleistocene produces ice-dammed proglacial lakes filling a large overdeepened subaerial basin in central Greenland during phases of deglaciation, with subglacial outlets in both the northwest and northeast (Keisling and others, 2020). Therefore, it could be plausible that sediments from these large proglacial lakes remain in this region, as such lakes interrupt the delivery of meltwater and sediment to proglacial zones, and act as highly efficient sediment traps (Carrivick and Tweed, 2013). Lake sediments have been shown to be preserved beneath the Laurentide Ice Sheet as well as beneath the ice sheet in northwest Greenland (Briner and others, 2007; Paxman and others, 2021).

A third sediment source is glacio-fluvial outwash, which may have been deposited in the interior at a time when erosive mountain valley glaciers were present as part of an ice mass restricted to the southern and eastern highlands, as is inferred to have existed during the late Miocene and/or Pliocene (Bierman and others, 2016; Paxman and others, 2024a). Some outlets of this modelled ice cap, which is geomorphologically and climatologically constrained (Paxman and others, 2024b), coincide directly with the upstream region, which generally sits lower than the surrounding topography, with the only possible outlet to the northwest (Fig. 7). Therefore, this region would have been a natural location for sediment being shed from the interior side of the eastern highlands to be accommodated, in front of the margin of an early highland ice cap. A comparable analogue for this mode of sediment deposition would be the Northern Patagonia Icefield, where outlet glaciers drain a large temperate icefield, terminating in proglacial lakes and forming glaciofluvial outwash plains (Glasser and others, 2009; Loriaux and Casassa, 2013).

4.1.2. Middle region

A distinct transition from the low roughness values (upstream region), to higher and more variable spatial roughness values (middle region), occurs at the topographic step which lies just downstream of the EastGRIP ice core site. This change marks the hypothesised limit of the sediment infill, as the rougher topography implies a discontinuity of the smooth sediments that lie upstream. This resembles findings at Pine Island Glacier and Thwaites Glacier (West Antarctica), where higher roughness relates to outcropping bedrock without significant sediment cover (Rippin and others, 2011; Schroeder and others, 2014). At this transitional zone between the upstream and middle regions of the NEGIS, the subglacial landscape comprises a mixed bed assemblage (Carter and others, 2025), where low roughness values coincide with sediment, and higher roughness relates to areas of bedrock outcrops, identified as crag and tails (Fig. 8). Areas of low roughness do occur again much further downstream, within the topographic low points of the large subglacial troughs (Fig. 5), which could suggest that sediments have also collected in these basins.

As well as rougher terrain, the middle region is characterised by the presence of two large subglacial troughs oriented in the direction of ice stream flow. These troughs are likely to be glacial in origin (Fig. 3), with classical *U*-shaped cross-sectional profiles and high width-to-depth ratios. Their linear structure suggests that these troughs potentially exploit inherited tectonic structures, such as a fault, as a line of geological weakness would act as a conduit for focused ice flow and selective erosion (Patton and others, 2016; Paxman and others, 2017). The effect of these troughs on the dynamics of the NEGIS is explored in further detail below.

4.1.3. Downstream region

There are distinct morphological similarities between the valleys in the downstream region of the NEGIS and those identified to the south in the eastern subglacial highlands (Paxman, 2023) (Fig. 3), such as their classification as highly 'glacial' in morphology, and comparable W/D ratios. The normally-distributed hypsometric curve is also characteristically alpine (Brocklehurst and Whipple, 2004; Jamieson and others, 2014), which can be clearly differentiated from the other two regions. This suggests that these landscapes had a common origin, meaning that the downstream region could comprise the outer, northernmost continuation of the eastern subglacial highlands, which were incised beneath erosive mountain glaciers during times of restricted ice extent (Paxman and others, 2024a). Some valleys underlying the NEGIS demonstrate slightly greater W/D ratios than the highlands; this could be attributed to subsequent continued erosion from the ice stream. A geological transition could also demarcate the middle and downstream regions, as the subglacial geology underlying the highlands has

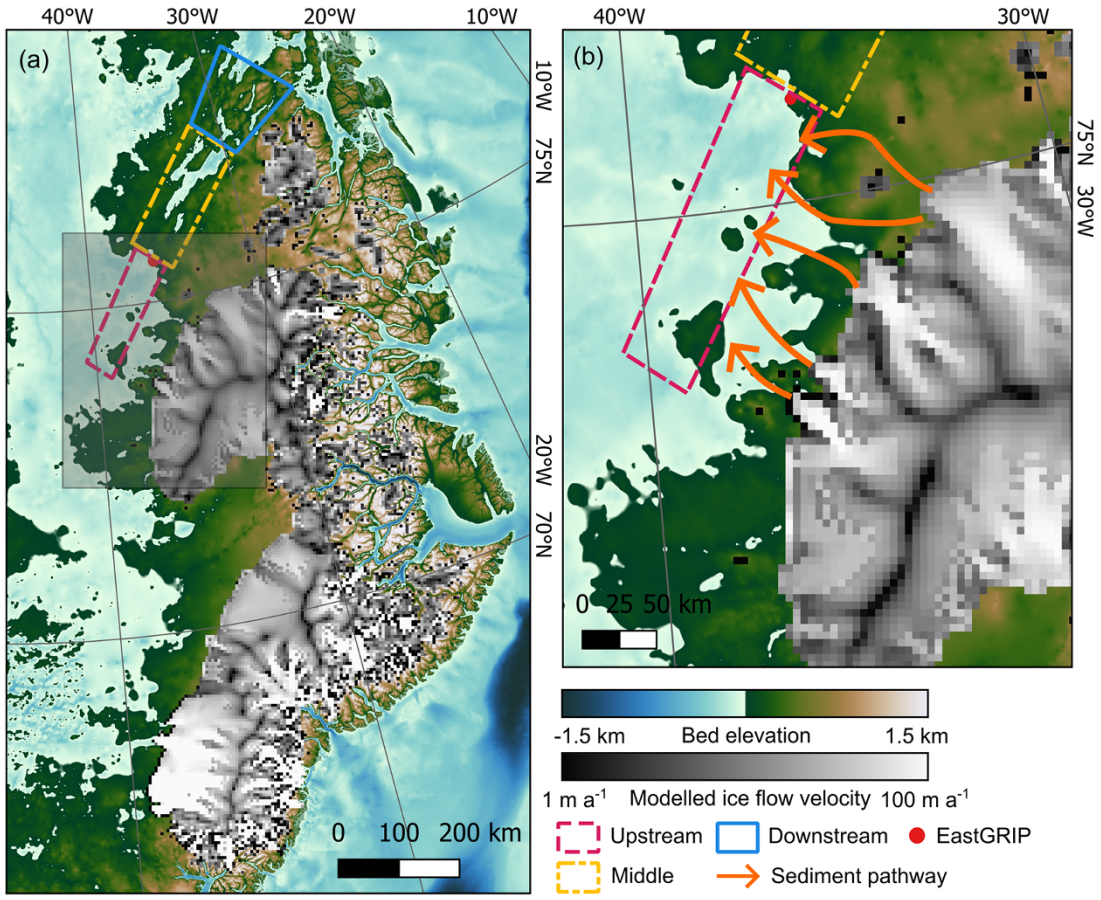

Figure 7. (a) Modelled ice cap present on the eastern subglacial highlands (constrained from the configuration of subglacial valley networks) during the past warmer climates (e.g. the late Miocene/Pliocene) (Paxman and others, 2024b). (b) Potential glaciofluvial sediment outwash pathways from the ice cap into the upstream region of the NEGIS.

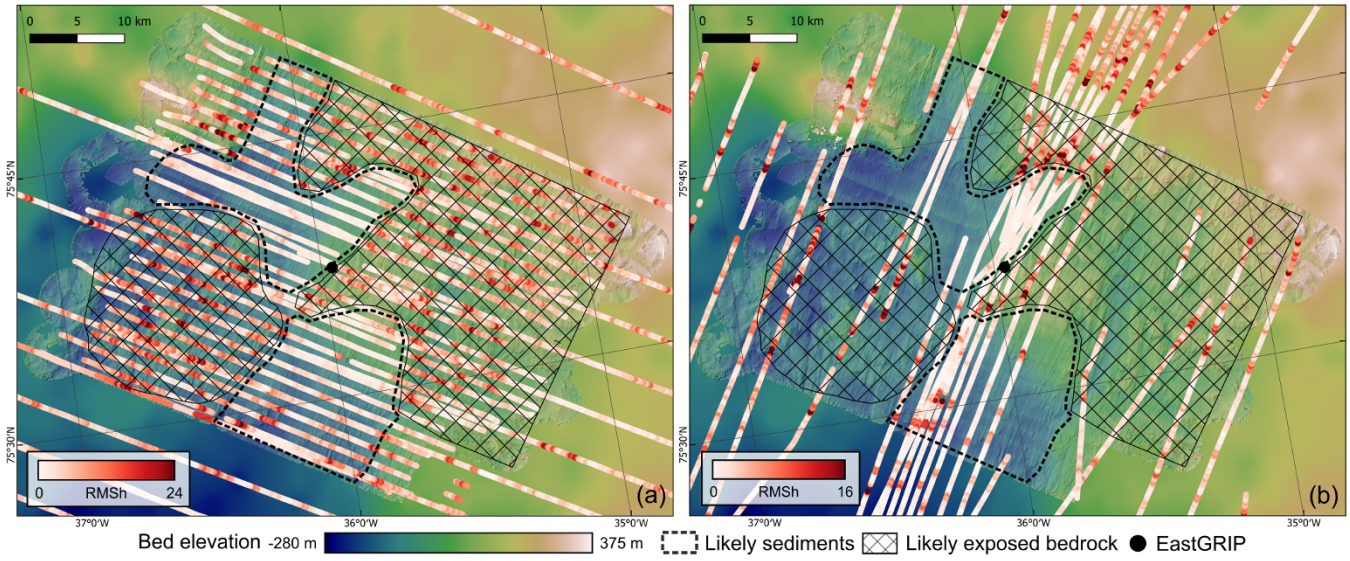

Figure 8. (a) Across- and (b) along-flow RMSh values overlain on high-resolution bed topography data generated from swath radar (Carter and others, 2025). Polygons delineate areas of likely sediments and exposed bedrock outcrops.

been identified as the Caledonian Orogen (MacGregor and others, 2024), and it would follow that the downstream region beneath the NEGIS represents the limit of this province.

4.2. Subglacial geological provinces

Greenland's subglacial geology, particularly beneath the interior of the ice sheet, is poorly constrained, and has been mostly derived

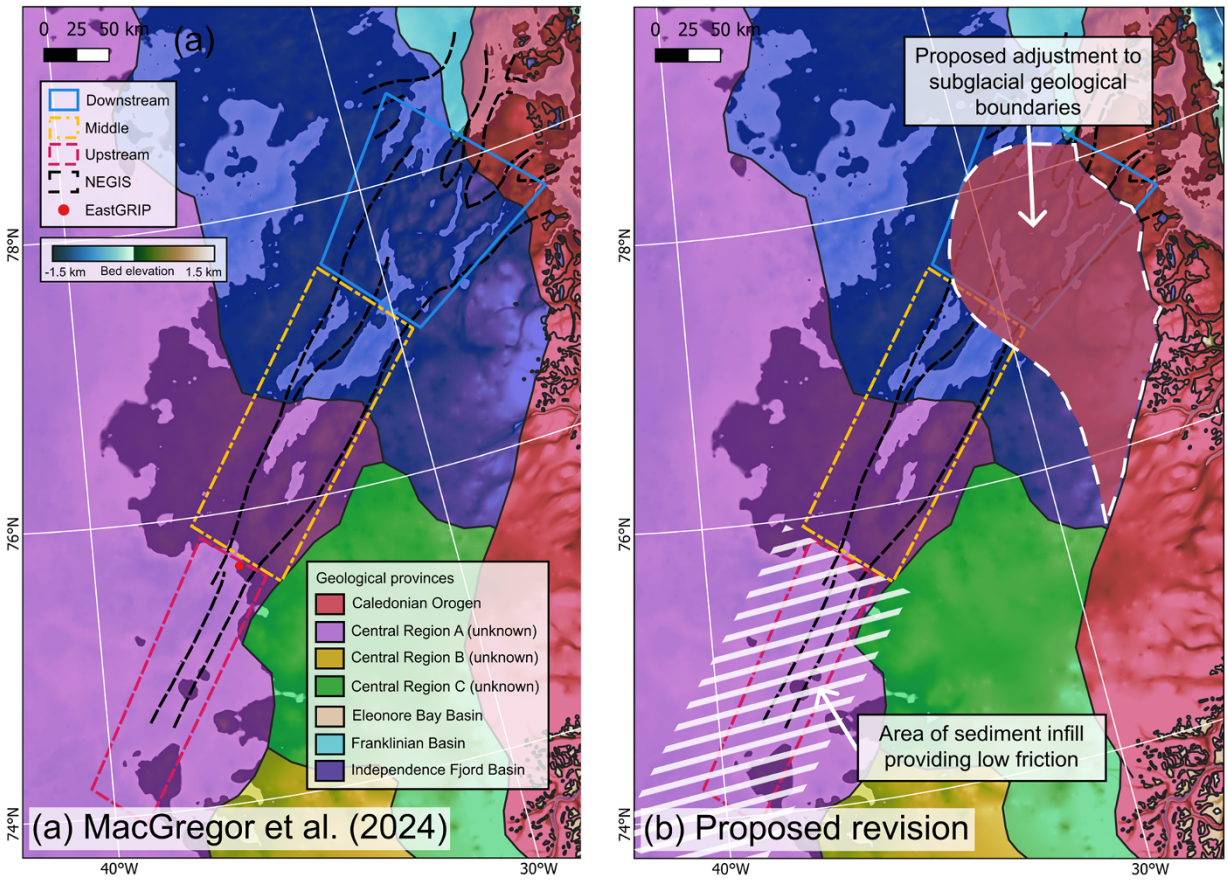

Figure 9. (a) Subglacial geological provinces that underlie the NEGIS (MacGregor and others, 2024), plotted over the subglacial topography (Morlighem and others, 2017). (b) The red area with a white dashed outline illustrates the proposed adjustment to the subglacial geological province boundaries, which would expand the area designated as the Caledonian Orogen to also underlie the downstream region. The white hashed area shows the region of sedimentary infill, which provides a low-friction subglacial environment.

from interpolation of geological mapping of its ice-free margins. MacGregor and others (2024) utilised geophysical data to improve upon previous mapping (Dawes, 2009), and refine the boundaries of its subglacial geological provinces. However, three subglacial regions were left unreconciled with marginal geology, one of which also underlies the NEGIS (Fig. 9a). The upstream and part of the middle region coincide with the unknown 'Central Region A', whereas the downstream region and other half of the middle region are proposed to be underlain by the Independence Fjord Basin (Fig. 9a). However, the exact positions of the province boundaries in this area are designated as 'low confidence' (MacGregor and others, 2024). Based on our new findings, we propose adjustments to these geological province boundaries, as the first-order differences in regional geomorphology beneath the NEGIS suggest varying geologies.

As highlighted above, the strong similarities of the valley morphology between the downstream region and eastern subglacial highlands may imply a common lithology. The abrupt transition from wider, shallower valleys in the middle region to relatively narrower and deeper valleys in the downstream region likely demarcates the geological boundary, as valley formation and morphology can be controlled by the underlying lithology. For example, in fluvial settings, valley width is two to three times wider in erosion-prone lithologies, such as sedimentary bedrock as compared to relatively erosion-resistant basalt (Schanz and Montgomery, 2016; Langston and Temme, 2019). Therefore, the clear difference in W/D ratio between the middle and downstream region is likely to be attributable to geological differences. Since the Caledonian Orogen underlies the highlands, we suggest that the subglacial province boundary should be modified so that the northern end of the Caledonian Orogen extends inland to incorporate the alpine-like topography of the downstream region of the NEGIS (Fig. 9b). Therefore, we suggest that the boundary between the Caledonian Orogen and Independence Fjord Basin coincides with the transition from the middle to downstream regions. We would also note here that the Independence Fjord sedimentary basin also differs from the unconsolidated sediments present in the upstream region, whilst also being distinct from the Caledonian Orogen, and might explain the presence of much larger subglacial troughs in the middle region due to its potentially greater erodibility.

4.3. *Relationship between bed geomorphology and ice dynamics*

At the onset of the NEGIS, bed morphology does not appear to have a controlling effect on the location of the shear margins, as the low roughness values do not vary significantly from within to outside of the ice stream in both the along- and across-flow directions. However, spatial topographic roughness beneath the NEGIS evolves downstream, with a distinct increase evident at the transition from the upstream to the middle region (Fig. 5), which could be interpreted to reflect the downstream limit of the sediment cover. This is opposite to what might be expected with increasing

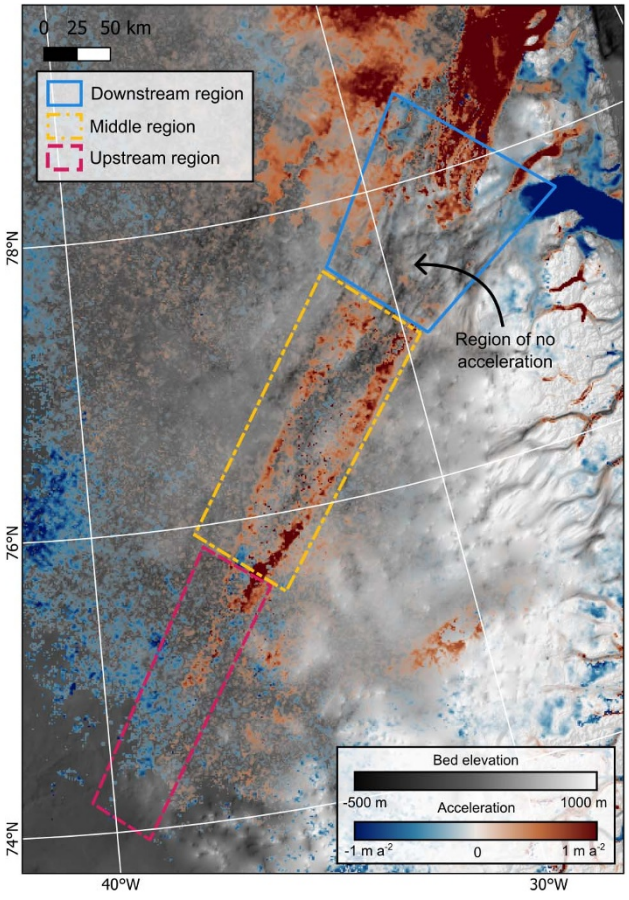

Figure 10. Recent dynamical acceleration of the NEGIS (Grinsted and others, 2022) overlying the subglacial topography. The disconnect between changes at the outlet glaciers and within the interior is evident as an area of zero acceleration in the downstream region. Values of zero acceleration are transparent in the colour scale.

ice flow velocity, as roughness often decreases with increasing flow speed (Rippin and others, 2011, 2014), and low roughness has been attributed to the facilitation of ice streaming and the presence of deformable sediment (Siegert and others, 2005; Rippin, 2013). However, increasing roughness values with increasing ice flow velocity have been observed to occur over a rough, hard bed, such as at the Institute and Möller Ice Streams, and Minch Palaeo-Ice Stream (Falcini and others, 2018). Fast ice flow, in the case of high roughness, could occur where there is a thick basal temperate ice layer, which would reduce drag (Krabbendam, 2016). An alternative explanation could also be an enhanced availability of water at the ice-bed interface, if the sediments in the upstream region act as an aquifer (Li and others, 2022), which terminates or discharges at the boundary between the upstream and middle regions.

Another significant controlling effect on the flow dynamics of the ice stream is the macroscale (10s of km) subglacial topography. To date, the NEGIS has been thought of as topographically unconstrained (Christianson and others, 2014; Holschuh and others, 2019; Franke and others, 2020), as the onset of the fast flow is not contained within a valley or trough. However, the large subglacial troughs in the middle region exert a clear influence on the flow dynamics of the ice stream, by channelling the fast flow towards the eastern side (Fig. 6). These valleys topographically steer the ice, but this focussing of faster flow occurs within the confines of the shear margins, which are themselves not contained by one all-encompassing valley or topographic 'low'. Even so, as ice can preferentially flow through the linear valleys in the middle region, the speed of that flow may propagate longitudinally upstream into the basin area, enabled by the low friction characteristics of the sedimentary basin which lies upstream (Fig. 9b). This could potentially explain the narrow band of fast flow experienced all the way inland, and the long, linear nature of the NEGIS, the shear margins of which are reinforced by directional hardening caused by the formation of anisotropic ice crystal orientation fabric (Gerber and others, 2023).

Another notable aspect of the NEGIS is its currently changing dynamic behaviour, as highlighted by its recent (last 35 a) acceleration, which has occurred both in the onset zone and its outlet glaciers (Grinsted and others, 2022; Khan and others, 2022). However, between the upper reaches of the NEGIS and its outlets near the ice margin, there is a distinct zone where surface velocities have not accelerated (Grinsted and others, 2022). This zone directly overlies the 'downstream region' mapped in this study, characterised by alpine-like topography (Fig. 10). Presently, it is unclear whether this is a coincidence or there are unknown causal mechanism(s) linking the spatial variation in bed topography and the dynamical changes of the ice. Nevertheless, the coincidence of the disconnection between the two areas where velocity has been observed to increase in recent decades (i.e. near the outlet and near the onset zone) and the spatial change in the characteristics of bed topography is clearly evident and requires further investigation.

5. Conclusions

In this study, we have investigated the detailed subglacial topography of the NEGIS, from its onset to where it splits into the three distinct outlet glaciers 79NG, ZI, and SG, to describe and demarcate three geomorphologically distinct regions beneath the ice stream. To ascertain the characteristics of the ice stream bed, we used the topographic analysis techniques of hypsometry, spatial roughness, and valley morphometry. In the upstream region at the onset of the ice stream, the low roughness, low relief, and lack of valleys indicate the presence of sediments. The origin of these sediments is unlikely to be marine incursion, but instead glaciofluvial outwash from an early ice cap on the eastern highlands (Paxman and others, 2024a) and/or proglacial lake infill (Keisling and others, 2020). A distinct transition to the middle region, with an abrupt increase in basal roughness, marks the downstream limit of this sediment infill. Two large, flow-parallel subglacial troughs characterise this middle region, which affect the ice stream geometry through topographic steering. Downstream, as the ice stream starts to diverge towards its current termini, the topography evolves again into smaller, alpine-like valleys, which are akin to the eastern subglacial highlands of Greenland. Here, we propose that the changes in valley morphometry are likely to be attributable to mechanical differences in the underlying geological provinces, as the morphological similarities between the downstream region and the adjacent eastern highlands would suggest that this downstream region is part of the Caledonian Orogenic Belt that comprises the highlands. This enables us to place an important constraint on the sub-ice geological structure of a region that was previously poorly understood.

Whilst the upstream regime appears to have little effect on the location of the onset of the ice stream and its shear margins, the downstream subglacial topography has a distinct impact on ice stream geometry, by preferentially steering ice flow through one

of the wide troughs. The low friction of the upstream regime may enable the propagation of fast ice flow longitudinally upstream, which could be one part of the explanation for the long, linear nature of the ice stream. On the basis of our data, we argue that the NEGIS is more influenced by basal topography than previously suggested.

Data availability statement. The OPR Toolbox is available at https://gitlab.com/openpolarradar/opr/. UWB radar data of the AWI UWB 2018 radar campaign is available on PANGAEA at https://doi.org/10.1594/PANGAEA.928569, and of the AWI UWB 2022 radar campaign at https://doi.org/10.1594/PANGAEA.986099. Bed picks from both AWI UWB radar campaigns are available on PANGAEA at https://doi.org/10.1594/PANGAEA.907918 (2018) and https://doi.pangaea.de/10.1594/PANGAEA.963555 (2022). Spatial roughness data (https://doi.org/10.1594/PANGAEA.984362) and valley classification results (https://doi.org/10.1594/PANGAEA.984371) are also available on PANGAEA. The upcoming BedMachine v.6 will include the bed elevation datapoints presented here.

Acknowledgements. The authors gratefully thank Mathieu Morlighem for incorporating the new AWI RES data from 2022 into a new version of BedMachine and for providing this dataset for analysis in this study. The authors thank the AWI polar aircraft technicians for their support in the field during the 2022 UWB radar flights as well as the Kenn Borek flight crew. For the NEGIS-FLOW airborne campaign, the authors acknowledge support via the AWI funding grant AWI_PA_02128. The authors thank the entire EastGRIP team during the 2022 field season for scientific and logistical support. EastGRIP is directed and organised by the Centre for Ice and Climate at the Niels Bohr Institute, University of Copenhagen. It is supported by funding agencies and institutions in Denmark (A. P. Møller Foundation, University of Copenhagen), USA (US National Science Foundation, Office of Polar Programs), Germany (Alfred Wegener Institute, Helmholtz Centre 475 for Polar and Marine Research), Japan (National Institute of Polar Research and Arctic Challenge for Sustainability), Norway (University of Bergen and Trond Mohn Foundation), Switzerland (Swiss National Science Foundation), France (French Polar Institute Paul-Emile Victor, Institute for Geosciences and Environmental research), Canada (University of Manitoba) and China (Chinese Academy of Sciences and Beijing Normal University). Furthermore, the authors acknowledge the use of software from Open Polar Radar generated with support from the University of Kansas, NASA grants 80NSSC20K1242 and 80NSSC21K0753, and NSF grants OPP-2027615, OPP-2019719, OPP-1739003, IIS-1838230, RISE-2126503, RISE-2127606, and RISE-2126468. The authors would like to thank Aspen Technology, Inc. for providing software licenses and support.

Author contributions. Charlotte M. Carter wrote the manuscript and conducted the main part of the data processing and analysis. Olaf Eisen and Daniela Jansen were PI and Co-I of the airborne campaigns. Daniela Jansen coordinated and conducted the fieldwork alongside John Paden. Charlotte M. Carter, Steven Franke, Guy J. G. Paxman, Stewart S. R. Jamieson, and Michael J. Bentley interpreted the radar and bed topography data. All co-authors discussed and commented on the manuscript.

Funding statement. Charlotte M. Carter was funded by the Alfred Wegener Institute's INSPIRES III programme. Steven Franke was funded by the Walter Benjamin Programme of the Deutsche Forschungsgemeinschaft (DFG, German Research Foundation; project number 506043073). Guy J. G. Paxman was supported by a Leverhulme Trust Early Career Fellowship (award number ECF-2021-549).

References

Arnold E and 6 others (2020) CReSIS airborne radars and platforms for ice and snow sounding. *Annals of Glaciology* **61**(81), 58–67. doi:10.1017/aog.2019.37

Alfred-Wegener-Institut Helmholtz-Zentrum für Polar- und Meeresforschung (2016) Polar aircraft Polar5 and Polar6 operated by the Alfred Wegener Institute. *Journal of Large-scale Research Facilities JLSRF* 2. doi:10.17815/jlsrf-2-153

Bamber JL, Siegert M, Griggs JA, Marshall SJ and Spada G (2013) Paleofluvial Mega-canyon beneath the Central Greenland Ice Sheet. *Science* **341**, 997–999. doi:10.1126/science.1239794

Bierman PR, Shakun JD, Corbett LB, Zimmerman SR and Rood DH (2016) A persistent and dynamic East Greenland ice sheet over the past 7.5 million years. *Nature* **540**(7632), 256–260. doi:10.1038/nature20147

Bingham RG and Siegert MJ (2007) Radar-derived bed roughness characterization of Institute and Möller ice streams, West Antarctica, and comparison with Siple Coast ice streams. *Geophysical Research Letters* **34**(21). doi:10.1029/2007gl031483

Bons PD and 8 others(2021) Comment on "Exceptionally high heat flux needed to sustain the Northeast Greenland Ice Stream" by Smith-Johnsen et al. (2020). *The Cryosphere* **15**(5), 2251–2254. doi:10.5194/tc-15-2251-2021

Briner JP, Axford Y, Forman SL, Miller GH and Wolfe AP (2007) Multiple generations of interglacial lake sediment preserved beneath the Laurentide Ice Sheet. *Geology* **35**(10). doi:10.1130/g23812a.1

Brocklehurst SH and Whipple KX (2004) Hypsometry of glaciated landscapes. *Earth Surface Processes and Landforms* **29**(7), 907–926. doi:10.1002/esp.1083

Carrivick JL and Tweed FS (2013) Proglacial lakes: Character, behaviour and geological importance. *Quaternary Science Reviews* **78**, 34–52. doi:10.1016/j.quascirev.2013.07.028

Carter CM and 6 others (2025) Formation of mega-scale glacial lineations far inland beneath the onset of the Northeast Greenland Ice Stream. *The Cryosphere* **19**, 5299–5315. doi:https://doi.org/10.5194/tc-19-5299-2025

Carter CM and 6 others (2023) Ice Thickness from downstream of the EastGRIP ice core site, North East Greenland Ice Stream, recorded with the airborne AWI UWB radar system. doi:10.1594/PANGAEA.963555

Christianson K and 7 others (2014) Dilatant till facilitates ice-stream flow in northeast Greenland. *Earth and Planetary Science Letters* **401**, 57–69. doi:10.1016/J.EPSL.2014.05.060

Chu W, Schroeder DM, Seroussi H, Creyts TT and Bell RE (2018) Complex basal thermal transition near the onset of Petermann Glacier, Greenland. *Journal of Geophysical Research: Earth Surface* **123**(5), 985–995. doi:10.1029/2017jf004561

Cooper MA, Jordan TM, Schroeder DM, Siegert MJ, Williams CN and Bamber JL (2019) Subglacial roughness of the Greenland Ice Sheet: Relationship with contemporary ice velocity and geology. *The Cryosphere* **13**(11), 3093–3115. doi:10.5194/tc-13-3093-2019

CReSIS (2024a) *2019_Greenland_P3 RDS Data*. Lawrence, Kansas, USA: Digital Media. http://data.cresis.ku.edu/

CReSIS (2024b) *1997_Greenland_P3, 1999_Greenland_P3, 2002_Greenland_P3, 2007_Greenland_P3, 2010_Greenland_DC8, 2012_Greenland_P3, 2013_Greenland_P3, 2014_Greenland_P3, 2015_Greenland_C130 RDS Data*. Lawrence, Kansas, USA: Digital Media. http://data.cresis.ku.edu/

Dawes PR (2009) The bedrock geology under the Inland Ice: The next major challenge for Greenland mapping. *Geological Survey of Denmark and Greenland Bulletin* **17**, 57–60.

Eisen O, Winter A, Steinhage D, Kleiner T and Humbert A (2020) Basal roughness of the East Antarctic Ice Sheet in relation to flow speed and basal thermal state. *Annals of Glaciology* **61**(81), 162–175. doi:10.1017/aog.2020.47

Fahnestock M, Abdalati W, Joughin I, Brozena J and Gogineni P (2001) High geothermal heat flow, basal melt, and the origin of rapid ice flow in central Greenland. *Science* **294**(5550), 2338–2342. doi:10.1126/science.1065370

Falcini FAM, Krabbendam M, Selby KA and Rippin DM (2021) Using bed-roughness signatures to characterise glacial landform assemblages beneath palaeo-ice sheets. *Journal of Glaciology* **68**(269), 518–532. doi:10.1017/jog.2021.122

Falcini FAM, Rippin DM, Krabbendam M and Selby KA (2018) Quantifying bed roughness beneath contemporary and palaeo-ice streams. *Journal of Glaciology* **64**(247), 822–834. doi:10.1017/jog.2018.71

Franke S and 11 others (2022a) Holocene ice-stream shutdown and drainage basin reconfiguration in northeast Greenland. *Nature Geoscience* **15**, 1–7. doi:10.1038/s41561-022-01082-2

Franke S and 6 others (2021) Complex basal conditions and their influence on ice flow at the onset of the Northeast Greenland Ice Stream. *Journal of Geophysical Research: Earth Surface* **126**(3). doi:10.1029/2020JF005689

Franke S and 7 others (2020) Bed topography and subglacial landforms in the onset region of the Northeast Greenland Ice Stream. *Annals of Glaciology* **61**(81), 143–153. doi:10.1017/aog.2020.12

Franke S and 7 others (2019) Bedrock topography and ice thickness in the onset region of the Northeast Greenland Ice Stream recorded with the airborne AWI Ultra-Wideband radar (UWB) in 2018. doi:10.1594/PANGAEA.907918

Franke S and 12 others (2022b) Airborne ultra-wideband radar sounding over the shear margins and along flow lines at the onset region of the Northeast Greenland Ice Stream. *Earth System Science Data* **14**(2), 763–779. doi:10.5194/essd-14-763-2022

Gardner A, Fahnestock M and Scambos TA (2022) MEaSUREs ITS_LIVE Regional Glacier and Ice sheet surface velocities V1. doi:10.5067/6II6VW8LLWJ7

Gerber TA and 22 others (2023) Crystal orientation fabric anisotropy causes directional hardening of the Northeast Greenland Ice Stream. *Nature Communications* **14**(1), 2653. doi:10.1038/s41467-023-38139-8

Glasser NF, Harrison S and Jansson KN (2009) Topographic controls on glacier sediment–landform associations around the temperate North Patagonian Icefield. *Quaternary Science Reviews* **28**(25-26), 2817–2832. doi:10.1016/j.quascirev.2009.07.011

Grinsted A and 8 others (2022) Accelerating ice flow at the onset of the Northeast Greenland Ice Stream. *Nature Communications* **13**(1). doi:10.1038/s41467-022-32999-2

Hale RD and 11 others (2016) Multi-channel ultra-wideband radar sounder and imager. *IGARSS*, 2112–2115. doi:10.1109/IGARSS.2016.7729545

Holschuh N, Lilien DA and Christianson K (2019) Thermal weakening, convergent flow, and vertical heat transport in the Northeast Greenland Ice Stream Shear Margins. *Geophysical Research Letters* **46**(14), 8184–8193. doi:10.1029/2019GL083436

Howat IM, Negrete A and Smith BE (2014) The Greenland Ice Mapping Project (GIMP) land classification and surface elevation data sets. *The Cryosphere* **8**(4), 1509–1518. doi:10.5194/tc-8-1509-2014

Jamieson SSR and 7 others (2014) The glacial geomorphology of the Antarctic ice sheet bed. *Antarctic Science* **26**(6), 724–741. doi:10.1017/s0954102014000212

Jansen D and 19 others (2024) Shear margins in upper half of Northeast Greenland Ice Stream were established two millennia ago. *Nature Communications* **15**(1), 1193. doi:10.1038/s41467-024-45021-8

Jeofry H and 8 others (2018) Hard rock landforms generate 130 km ice shelf channels through water focusing in basal corrugations. *Nature Communications* **9**(1), 4576. doi:10.1038/s41467-018-06679-z

Joughin I, Fahnestock M, Macayeal D, Bamber JL and Gogineni P (2001) Observation and analysis of ice flow in the largest Greenland ice stream. *Journal of Geophysical Research: Atmospheres* **106**(D24), 34021–34034. doi:10.1029/2001jd900087

Karlsson NB and Dahl-Jensen D (2015) Response of the large-scale subglacial drainage system of Northeast Greenland to surface elevation changes. *The Cryosphere* **9**(4), 1465–1479. doi:10.5194/tc-9-1465-2015

Keisling BA, Nielsen LT, Hvidberg CS, Nuterman R and Deconto RM (2020) Pliocene–Pleistocene megafloods as a mechanism for Greenlandic megacanyon formation. *Geology* **48**(7), 737–741. doi:10.1130/g47253.1

Khan SA and 9 others (2022) Extensive inland thinning and speed-up of Northeast Greenland Ice Stream. *Nature* **2022**, 1–6. doi:10.1038/s41586-022-05301-z

Krabbendam M (2016) Sliding of temperate basal ice on a rough, hard bed: Creep mechanisms, pressure melting, and implications for ice streaming. *The Cryosphere* **10**(5), 1915–1932. doi:10.5194/tc-10-1915-2016

Krieger L, Floricioiu D and Neckel N (2019) Drainage basin delineation for outlet glaciers of Northeast Greenland based on Sentinel-1 ice velocities and TanDEM-X elevations. *Remote Sensing of Environment*, 237. doi:10.1016/j.rse.2019.111483

Langston AL and Temme AJAM (2019) Impacts of lithologically controlled mechanisms on downstream bedrock valley widening. *Geophysical Research Letters* **46**(21), 12056–12064. doi:10.1029/2019gl085164

Li L, Aitken ARA, Lindsay MD and Kulessa B (2022) Sedimentary basins reduce stability of Antarctic ice streams through groundwater feedbacks. *Nature Geoscience* **15**(8), 645–650. doi:10.1038/s41561-022-00992-5

Loriaux T and Casassa G (2013) Evolution of glacial lakes from the Northern Patagonia Icefield and terrestrial water storage in a sea-level rise context. *Global and Planetary Change* **102**, 33–40. doi:10.1016/j.gloplacha.2012.12.012

MacGregor JA and 45 others (2021) The scientific legacy of NASA's Operation Icebridge. *Reviews of Geophysics* **59**(2). doi:10.1029/2020rg000712

MacGregor JA and 10 others (2024) Geologic provinces beneath the Greenland Ice Sheet constrained by geophysical data synthesis. *Geophysical Research Letters* **51**(8). doi:10.1029/2023gl107357

Morlighem M and 31 others (2022) IceBridge BedMachine Greenland, version 5. doi:10.5067/GMEVBWFLWA7X

Morlighem M and 31 others (2017) BedMachine v3: Complete bed topography and ocean bathymetry mapping of greenland from multibeam echo sounding combined with mass conservation. *Geophysical Research Letters* **44**(21), 11051–11061. doi:10.1002/2017GL074954

Munevar Garcia S, Miller LE, Falcini FAM and Stearns LA (2023) Characterizing bed roughness on the Antarctic continental margin. *Journal of Glaciology*, 1–12. doi:10.1017/jog.2023.88

Patton H, Swift DA, Clark CD, Livingstone SJ and Cook SJ (2016) Distribution and characteristics of overdeepenings beneath the Greenland and Antarctic ice sheets: Implications for overdeepening origin and evolution. *Quaternary Science Reviews* **148**, 128–145. doi:10.1016/J.QUASCIREV.2016.07.012

Paxman GJG (2023) Patterns of valley incision beneath the Greenland Ice Sheet revealed using automated mapping and classification. *Geomorphology*, 436. doi:10.1016/j.geomorph.2023.108778

Paxman GJG, Austermann J and Hollyday A (2022a) Total isostatic response to the complete unloading of the Greenland and Antarctic Ice Sheets. *Scientific Reports* **12**(1). doi:10.1038/s41598-022-15440-y

Paxman GJG, Austermann J and Hollyday A (2022b) Grid files of the total isostatic response to the complete unloading of the Greenland and Antarctic Ice Sheets (version 2). doi:10.18739/A2WS8HN3C

Paxman GJG, Austermann J and Tinto KJ (2021) A fault-bounded palaeolake basin preserved beneath the Greenland Ice Sheet. *Earth and Planetary Science Letters* **553**. doi:10.1016/j.epsl.2020.116647

Paxman GJG, Jamieson S, Dolan AM and Bentley MJ (2024b) Subglacial valleys preserved in the highlands of south and east Greenland record restricted ice extent during past warmer climates: Datasets (2.0). doi:10.5281/zenodo.10649455

Paxman GJG, Jamieson SSR, Dolan AM and Bentley MJ (2024a) Subglacial valleys preserved in the highlands of south and east Greenland record restricted ice extent during past warmer climates. *The Cryosphere* **18**(3), 1467–1493. doi:10.5194/tc-18-1467-2024

Paxman GJG and 8 others (2017) Uplift and tilting of the Shackleton Range in East Antarctica driven by glacial erosion and normal faulting. *Journal of Geophysical Research: Solid Earth* **122**(3), 2390–2408. doi:10.1002/2016jb013841

Rippin DM (2013) Bed roughness beneath the Greenland ice sheet. *Journal of Glaciology* **59**(216), 724–732. doi:10.3189/2013jog12j212

Rippin DM, Bamber JL, Siegert MJ, Vaughan DG and Corr HFJ (2006) Basal conditions beneath enhanced-flow tributaries of Slessor Glacier, East Antarctica. *Journal of Glaciology* **52**(179), 481–490. doi:10.3189/172756506781828467

Rippin DM and 9 others (2014) Basal roughness of the Institute and Möller Ice Streams, West Antarctica: Process determination and landscape interpretation. *Geomorphology* **214**, 139–147. doi:10.1016/j.geomorph.2014.01.021

Rippin DM, Vaughan DG and Corr HFJ (2011) The basal roughness of Pine Island Glacier, West Antarctica. *Journal of Glaciology* **57**(201), 67–76. doi:10.3189/002214311795306574

Riverman KL and 8 others (2019) Wet subglacial bedforms of the NE Greenland Ice Stream shear margins. *Annals of Glaciology* **60**(80), 91–99. doi:10.1017/aog.2019.43

Roberts DH and 15 others (2024) The deglacial history of 79N Glacier and the Northeast Greenland Ice Stream. *Quaternary Science Reviews* **336**. doi:10.1016/j.quascirev.2024.108770

Rodriguez-Morales F and 17 others (2014) Advanced multifrequency radar instrumentation for polar research. *IEEE Transactions on Geoscience and Remote Sensing* **52**(5), 2824–2842. doi:10.1109/tgrs.2013.2266415

Rysgaard S, Bendtsen J, Mortensen J and Sejr MK (2018) High geothermal heat flux in close proximity to the Northeast Greenland Ice Stream. *Scientific Reports* **8**(1). doi:10.1038/s41598-018-19244-x

Schanz SA and Montgomery DR (2016) Lithologic controls on valley width and strath terrace formation. *Geomorphology* **258**, 58–68. doi:10.1016/j.geomorph.2016.01.015

Schroeder DM, Blankenship DD, Young DA, Witus AE and Anderson JB (2014) Airborne radar sounding evidence for deformable sediments and outcropping bedrock beneath Thwaites Glacier, West Antarctica. *Geophysical Research Letters* **41**(20), 7200–7208. doi:10.1002/2014gl061645

Siegert MJ and 7 others (2016) Subglacial controls on the flow of Institute Ice Stream, West Antarctica. *Annals of Glaciology* **57**(73), 19–24. doi:10.1017/aog.2016.17

Siegert MJ, Taylor J and Payne AJ (2005) Spectral roughness of subglacial topography and implications for former ice-sheet dynamics in East Antarctica. *Global and Planetary Change* **45**(1-3), 249–263. doi:10.1016/j.gloplacha.2004.09.008

Smith BE, Raymond CF and Scambos T (2006) Anisotropic texture of ice sheet surfaces. *Journal of Geophysical Research: Earth Surface* **111**(F1). doi:10.1029/2005jf000393

Smith MW (2014) Roughness in the Earth Sciences. *Earth-Science Reviews* **136**, 202–225. doi:10.1016/j.earscirev.2014.05.016

Smith-Johnsen S, de Fleurian B, Schlegel N, Seroussi H and Nisancioglu K (2020) Exceptionally high geothermal heat flux needed to sustain the Northeast Greenland Ice Stream. *The Cryosphere* **14**, 841–854. doi:10.5194/tc-14-841-2020

Studinger M and 7 others (2001) Subglacial sediments: A regional geological template for ice flow in West Antarctica. *Geophysical Research Letters* **28**(18), 3493–3496. doi:10.1029/2000gl011788

Winsborrow MCM, Clark CD and Stokes CR (2010) What controls the location of ice streams? *Earth-Science Reviews* **103**(1-2), 45–59. doi:10.1016/j.earscirev.2010.07.003

Appendix A

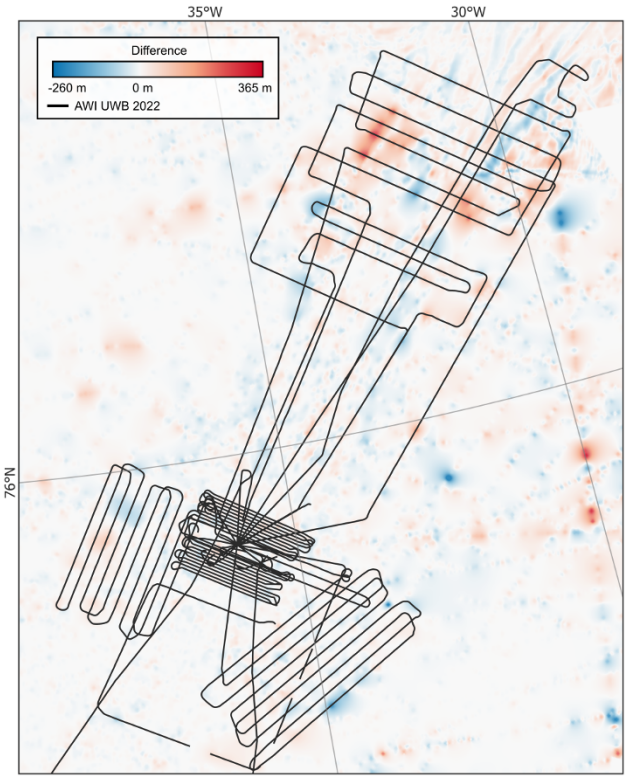

Figure A1. Difference (v5 minus v6.2) in elevation between BedMachine v5 (Morlighem and others, 2022) and the updated BedMachine v6.2, which includes the new bed elevation data obtained from the AWI UWB 2022 flightlines (black lines).